BRIEF REPORT

Impulsivity Markers in Parkinsonian Subthalamic Single-Unit Activity

Federico Micheli, MSc,[1,2,†] Matteo Vissani, MSc,[1,2,†] Guido Pecchioli, MD,[3] Federica Terenzi, MD,[4] Silvia Ramat, MD, PhD,[3] and Alberto Mazzoni, PhD[1,2*]

[1]*The Biorobotics Institute, Scuola Superiore Sant'Anna, Pisa, Italy* [2]*Department of Excellence in Robotics and AI, Scuola Superiore Sant'Anna, Pisa, Italy* [3]*Dipartimento Neuromuscolo-Scheletrico e degli Organi di Senso, AOU Careggi, Florence, Italy* [4]*Dipartimento di Neuroscienze, Psicologia, Università degli Studi di Firenze, Area del Farmaco e Salute del Bambino, Florence, Italy*

ABSTRACT: Background: Impulsive-compulsive behaviors are common in Parkinson's disease (PD) patients. However, the basal ganglia dysfunctions associated with high impulsivity have not been fully characterized. The objective of this study was to identify the features associated with impulsive-compulsive behaviors in single neurons of the subthalamic nucleus (STN).

Methods: We compared temporal and spectral features of 412 subthalamic neurons from 12 PD patients with impulsive-compulsive behaviors and 330 neurons from 12 PD patients without. Single-unit activities were extracted from exploratory microrecordings performed during deep brain stimulation (DBS) implant surgery in an OFF medication state.

Results: Patients with impulsive-compulsive behaviors displayed decreased firing frequency during bursts and a larger fraction of tonic neurons combined with weaker beta coherence. Information carried by these features led to the identification of patients with impulsive-compulsive behaviors with an accuracy greater than 80%.

Conclusions: Impulsive-compulsive behaviors in PD patients are associated with decreased bursts in STN neurons in the OFF medication state. © 2021 International Parkinson and Movement Disorder Society

***Correspondence to:** Dr. Alberto Mazzoni, The Biorobotics Institute of Scuola Superiore Sant'Anna, Viale Rinaldo Piaggio 34, Pontedera, Pisa, Italy; E-mail: alberto.mazzoni@santannapisa.it

Federico Micheli and Matteo Vissani share the same first-author contribution.

Relevant conflicts of interest/financial disclosures: Nothing to report.

Funding agencies: The research was supported in part by the Italian Ministry of Research (MIUR, PRIN2017, PROTECTION, project 20178L7WRS). All the authors declare that they have not received other funds from any institution, including personal relationships, interests, grants, employment, affiliations, patents, inventions, honoraria, consultancies, royalties, stock options/ownership, or expert testimony in the last 12 months.

Received: 1 July 2020; **Revised:** 14 December 2020; **Accepted:** 21 December 2020

Published online in Wiley Online Library (wileyonlinelibrary.com). DOI: 10.1002/mds.28497

Parkinson's disease (PD) is characterized by motor dysfunctions such as tremor, bradykinesia, rigidity, and axial symptoms. However, following dopamine agonist (DA) therapy, more than 25% of patients with PD display impulsive-compulsive behaviors (ICB)[1] based on seeking immediate rewards,[2-4] such as pathological gambling, shopping, binge eating, and hypersexuality. Dopamine replacement treatment, especially DA agents, is a major risk factor for developing impulse control disorders,[5] whereas the relationship with deep brain stimulation (DBS) has not been entirely elucidated.[6]The neural substrate of impulsivity is still unknown. Structures involved in impulse control disorders include the ventral striatum, prefrontal cortex, anterior cingulate, and subthalamic nucleus (STN),[7] which has inhibitory control in conflictual decisions.[8] This role of the STN is consistent with the involvement of the corticobasal ganglia circuits in proactive and reactive inhibition of movement and cognition.[8,9] Markers of impulse control disorders were found in the STN of PD patients during rest[10] and risk decision tasks.[11,12] However, a full understanding of the underlying activity at the single neuron level is still missing. Here, we investigate the possibility of identifying subjects displaying ICB with microelectrode recordings (MERs)[13] performed at rest for target identification during DBS implant surgery. We analyzed MERs acquired during STN-DBS implant surgery in 12 PD patients with diagnosed ICB (ICB+) and 12 PD patients without ICB (ICB−). We found relevant differences between the 2 conditions in the features of single-neuron activity.

Patients and Methods

Patients

This study was conducted in accordance with the Declaration of Helsinki and after ethical approval (Careggi Hospital, Florence, Italy). We retrospectively included 24 PD patients from our movement disorders outpatient clinic (7 women; age at DBS, 62 years [59–66.5 years]; PD duration, 12.5 years [8.5–16 years]; medians and 25th–75th percentiles are reported for the whole subsection). Inclusion criteria were diagnosis of

PD according to the Parkinson's Disease UK Brain Bank for idiopathic Parkinson's disease[14] and previous treatment with bilateral STN-DBS. A subgroup of 12 patients (3 women; age at DBS, 62.5 years [52–65 years]; PD duration, 11 years [8.5–18.5 years]) was diagnosed with at least 1 current ICB (Supplementary Methods). The 2 subgroups (ICB– vs ICB+) did not significantly differ in motor severity scales or dopaminergic therapy (Table S1) but did differ in Barratt Impulsiveness Scale (BIS),[15] 53.7 ± 2.8 versus 65.8 ± 4.8; *t* test, $P = 0.001$. All patients were operated on at Careggi Hospital Florence, Florence, Italy. Anatomical localization of the STN was performed using T2, SWI, and T1 sequences of the preoperative 1.5-T MRI fused with preoperative stereotactic CT scan (with Leksell G frame) assisted by StealthStation (Medtronic Inc., Minneapolis, MN). Intraoperative STN targeting was optimized by microelectrode recordings and clinical test stimulation. Patients were recorded when the dopaminergic medication was OFF.

Surgical Procedure and Electrophysiological Recordings

Surgery was performed using a stereotactic frame-based procedure with intraoperative MER and macrostimulation for STN targeting. Implantation of the quadripolar DBS electrodes (model 3389; Medtronic) was performed bilaterally under local

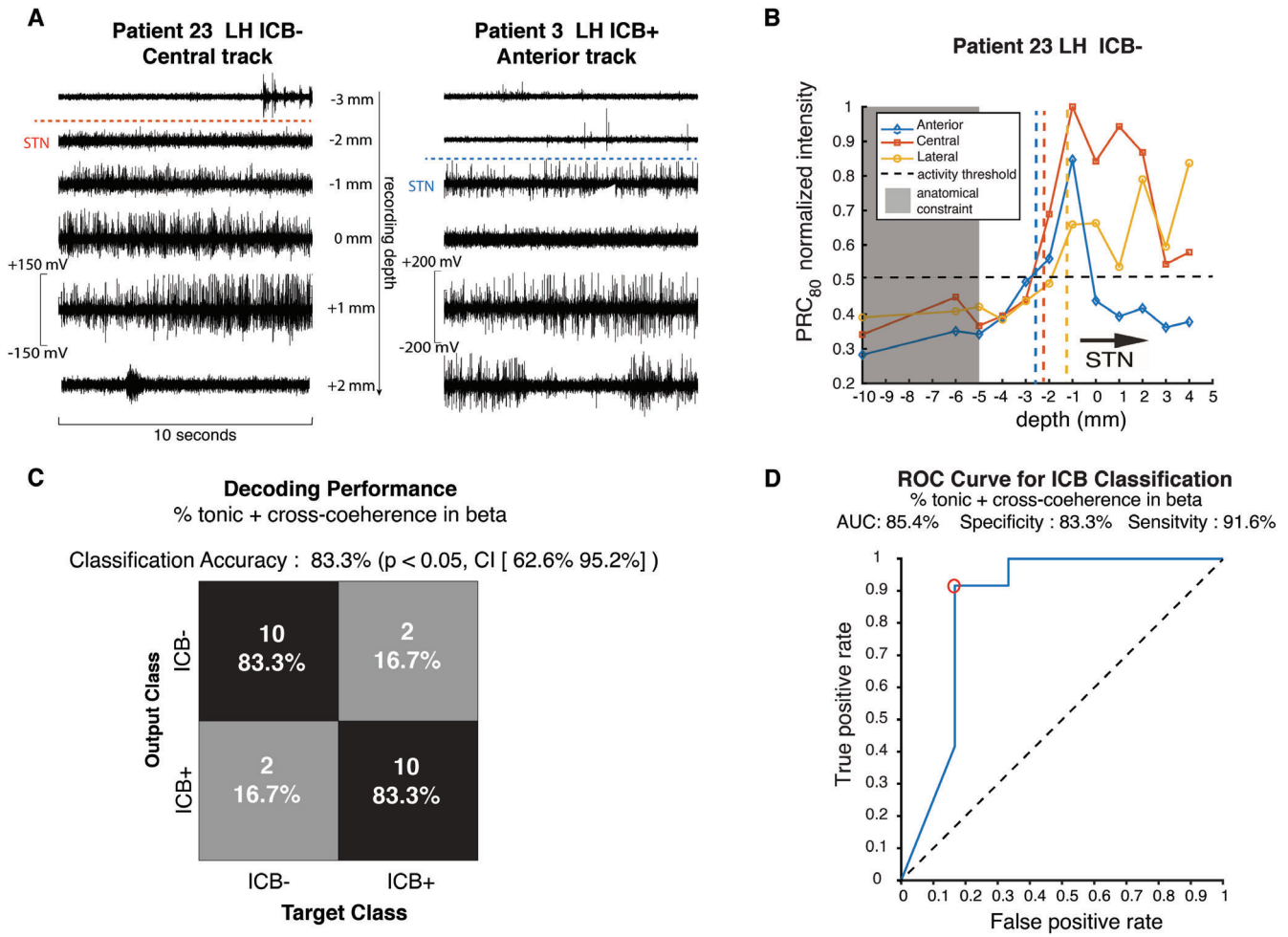

FIG. 1. (**A**) Intraoperative microelectrode recordings from a representative ICB– patient, patient 23 (left), and from a representative ICB+ patient, patient 3 (right), across depths (0 mm indicates clinical target). Color dashed lines represent the entry point of the track in the STN (see Methods and B). (**B**) STN depth range identification method. The 80th percentile of the raw recording (PRC80) relative intensity (see Methods) across depths for the 3 tracks of the left hemisphere insertion of patient 23. The horizontal black dashed line represents the activity threshold set to 50% of the maximum PRC80 intensity value. The gray patch represents the anatomical constraint to consider a recording in the STN (each recording above "–5 mm" relative to the target position was excluded). Blue, red, and yellow vertical dashed lines represent the STN entrance point for anterior, central, and lateral tracks, respectively. Only recordings beyond this depth, for which the PRC80 value was above the activity threshold, were considered to belong to the STN (eg, only 2 recordings for the anterior track in the plot). (**C**) Performance of the support vector machine (SVM) classifier with 2 combined neural features (n = 24; see Methods).The 95% confidence interval was calculated with the Clopper–Pearson method for a binomial distribution. (**D**) Receiver operating characteristic (ROC) curve for ICB classification in C. The red circle indicates the "optimal operating point." Specificity and sensitivity were reported for the optimal point. The dashed line represents the identity. [Color figure can be viewed at wileyonlinelibrary.com]

TABLE 1. Discrimination performance of single neural features

Neural features		Population-level: Cohen's d (*P*, MWUt) Information			Patient-level classification accuracy (confidence interval) [AUC/specificity/sensitivity]		
Class	Feature	ICB− vs ICB+	Weak motor symptoms vs strong motor symptoms	Tremor-dominant vs Brady-dominant	ICB− vs ICB+	Weak motor symptoms vs strong motor symptoms	Tremor-dominant vs Brady-dominant
Firing pattern	Firing rate	−0.11 (*P* = 0.15) 0.001 bits	0.14 (*P* = 0.09) 0.004 bits	0.02 (*P* = 0.09) 0.004 bits	58% (33.3–66.7) [61.8%/68%/52.6%]	59.8% (37.5–70.8) [54.5%/68%/54.3%]	48.7% (25–54.2) [50%/0%/100%]
	Percent tonic neurons	22.1% vs 30.8% **P = 0.029** (Fisher's exact test) **0.006 bits**	26.0% vs 27.8% *P* = 0.74 (Fisher's exat test) 0 bits	26.2% vs 27.5% *P* = 0.74 (Fisher's exact test) 0 bits	**70.5% (66.7–70.8)** [75.2%/58%/91.7%]	38.6% (20.8–54.2) [33.2%/100%/0%]	46.8% (20.8–54.2) [41.3%/0%/100%]
Bursting activity	Intraburst frequency	**0.23** **(P = 0.014)** **0.008 bits**	0.04 (*P* = 0.92) 0.002 bits	**0.17** **(P < 0.014)** **0.008 bits**	**74.2% (58.3–79.2)** [68.2%/72%/77.1%]	43.4% (25–54.2) [33.4%/92%/12.6%]	55.7% (41.7–66.7) [54.4%/42%/70.5%]
	Interburst interval	0.03 (*P* = 0.52) 0 bits	−0.04 (*P* = 0.55) **0.0065 bits**	0.12 (*P* = 0.23) **0.007 bits**	40.2% (16.7–62.5) [34.6%/100%/0%]	44% (16.7–58.3) [40.2%/94%/9.2%]	50.9% (29.2–62.5) [38.8%/0%/100%]
	Duration	−0.11 (*P* = 0.35) 0 bits	0.15 (*P* = 0.31) 0 bits	0.02 (**P** = 0.24) 0.004 bits	51.6% (29.2–62.5) [52.3%/68%/41.4%]	46% (33.3–58.3) [38.3%/100%/1.2%]	52.7% (37.5–58.3) [31.5%/2%/99%]
Oscillatory activity Delta (1–4 Hz) Theta (4–8 Hz) Alpha (8–12 Hz) Beta (12–30 Hz) Gamma (30–100 Hz)	SUA-BUA coherence in theta band	0.01 (*P* = 0.68)	−0.30 (*P* = 0.07)	0.20 (*P* = 0.27)	45.9% (25–58.3) [45.4%/28%/86.9%]	**68.6% (62.5–79.2)** [76.4%/54%/98.8%]	47% (25–58.3) [43%/0%/100%]
	SUA-BUA coherence in beta band	0.29 (*P* = 0.07) 0.01 bits	−0.09 (*P* = 0.45) 0.003 bits	−0.15 (*P* = 0.49) 0 bits	**63.1% (54.2–70.8)** [66.4%/90%/41.8%]	47.6% (20.8–62.5) [53.3%/18%/99%]	56% (41.7–66.7) [50.8%/20%/93.2%]
	BUA power in delta band	0.09 (*P* = 0.34) 0 bits	0.33 **(P = 0.014)** 0.018 bits	−0.01 (*P* = 0.88) 0 bits	48.3% (33.3–62.5) [45.9%/100%/4.9%]	**66% (58.3–0.708)** [68.3%/80%/55.3%]	48.5% (29.2–0.583) [37.7%/0%/100%]
	BUA power in theta band	−0.09 (*P* = 0.42) 0.004 bits	0.13 (*P* = 0.33) 0.001 bits	−0.03 (*P* = 0.45) **0.01 bits**	45.5% (20.8–62.5) [43.5%/50%/57.5%]	41.8% (25–62.5) [38.3%/100%/0%]	49.3% (29.2–54.2) [48%/0%/100%]
	BUA power in alpha band	−0.11 (*P* = 0.45) 0 bits	0.04 (*P* = 0.88) 0 bits	0.11 (*P* = 0.34) 0.002 bits	45% (29.2–62.5) [37.6%/100%/0%]	42.6% (29.2–58.3) [35.5%/8%/93.6%]	51.6% (41.7–62.5) [48.9%/2%/99.9%]
	BUA power in beta band	0.41 **(P < 0.001)** **0.019 bits**	0.23 **(P = 0.04)** **0.01 bits**	0.18 **(P < 0.02)** **0.012 bits**	**65.9% (58.3–70.8)** [64.5%/48%/91%]	54.8% (25–70.8) [54.8%/60%/61%]	49.8% (33.3–58.3) [46.6%/2%/99.5%]
	BUA power in gamma band	−0.13 (*P* = 0.06) **0.016 bits**	0.3 **(P < 0.013)** **0.01 bits**	0.06 (*P* = 0.06) **0.016 bits**	50.1% (29.2–62.5) [41.7%/92%/15.8%]	51.5% (29.2–62.5) [50.7%/86%/22%]	48.3% (37.5–62.5) [50.8%/18%/88.4%]

Comparison of the efficacy of single neural features in discriminating between (1) ICB− and ICB+ condition, (2) weak and strong motor symptoms (UPDRS median split; see Methods), (3) bradykinetic-rigid or tremor-dominant phenotype. Each row corresponds to a neural feature (second column) belonging to a given class (first column) and reports (1) intergroup difference (measured with Cohen's d effect size and tested with Mann–Whitney *U* test [MWUt] except for % of tonic neurons tested with Fisher exact test) and information carried about the condition over all 742 neurons (population-level discrimination, columns 3 to 5), (2) performance in classifying the condition of each patient according to the average value of the feature over all neurons of the patient and area under the curve (AUC) specificity and sensitivity of classification (patient level classification, columns 6 to 8). Significant results (see Methods) are reported in bold.

anesthesia with 2% lidocaine and bupivacaine. Electrophysiological recordings started at 10 mm above the target location identified through stereotactic imaging and were performed using a Medtronic lead-point system (Medtronic) using 3 tracks: anterior, central, and lateral. An exploratory trajectory was followed by extruding the microelectrode (250 lm tip, impedance 1–1.5 MX; FHC Inc., Bowdoinham ME). Microrecording tracks were performed with 0.5-mm steps. Each recording lasted at least 10 seconds. Signals were acquired at 24 kHz and high-pass-filtered with a hardware filter at 200 Hz to remove low frequencies and allow for the visualization of firing neuronal activity during surgery (see Fig. 1A). Afterward, an implanted pulse generator was fixed to the DBS electrodes under general anesthesia.

STN Entry Point Identification

The first step of off-line recording analysis was the identification of STN recordings.[16] Recordings were considered to belong to the STN if they: (1) were deeper than −5 mm, (2) presented an 80th percentile of the raw recording (PRC80) ≥ 50% of the highest value (Fig. 1B, Supplementary Methods).

Spike Detection and Neural Marker Estimation

We sorted the single-unit activity (SUA) using MATLAB ToolBox Wave Clus,[17,18] extracting 742 SUA (330 SUA in the ICB− group and 412 in the ICB+ group) from 548 tracks across all subjects. From the SUA, we extracted the neural features associated with firing patterns and bursting activity: firing rate[19] and fraction of tonic neurons.[18] Intraburst frequency (IBF), interburst interval, and total bursting duration were computed[20] and averaged over each SUA. We then analyzed the background unit activity (BUA), that is, the raw signal once action potentials were removed, computing its spectral density with standard bands and oscillatory SUA-BUA coherence.[21] Full details are reported in Supplementary Methods.

Statistical Analysis

Neural features were first compared between the ICB+ and ICB− groups using the population-level approach, that is pooling all neurons/channels from each group. We computed each feature's information content about the ICB+ condition, and both BIS and UPDRS scales were modeled in a general linear model using selected neural features (see Supplementary Methods).

Classification Performance

We assessed the ability of each feature in identifying ICB+ patients with a linear support vector machine (SVM) classifier. Each feature was averaged across SUA for each patient and *z*-scored across patients of both groups. The SVM classifier was trained and tested with 4-fold cross-validation. Scores for the classification of each patient were obtained as the percentage of correct classifications after 100 runs of the classifier and used to compute the receiver operating characteristic (ROC) performance curve, the area under the curve (AUC), and the specificity and sensitivity for optimal threshold. This analysis was repeated for all pairwise combinations of features with significant differences in the population-level comparison and belonging to 2 different neural feature categories (Table 1). Statistical and classification analyses were repeated to divide patients into (1) lower versus higher UPDRS score groups (median-split) and (2) bradykinetic-rigid or tremor-dominant groups.

Results

We evaluated the differences at the neural population level between the ICB+ and ICB− conditions using a broad spectrum of neural features, divided into 3 classes: firing patterns, bursting activity, and oscillatory activity (see Patients and Methods). The fraction of tonic neurons, IBF, and BUA beta and gamma power displayed significant population differences across conditions and carried significant information about the ICB+ condition (see Table 1 and Patients and Methods). For each feature, an SVM classifier discriminated at a single patient level between the ICB− and ICB+ conditions (see Patients and Methods). The highest single feature discrimination accuracy was achieved using IBF (79.2%; 95% CI, 57.9%–92.9%; Table 1). In stark contrast, IBF was unable to discriminate between weak or strong motor symptoms or motor phenotypes (see Table 1). IBF was also a significant predictor of BIS (R^2 = 0.224, P = 0.019) but not of UPDRS (R^2 = 0.001, P = 0.906). Combining the fraction of tonic neurons and SUA-BUA beta coherence (see Patients and Methods) led to accuracy at the patient level of 83.3% (20 of 24; 95% CI, 62.6%–95.2%; Fig. 1C). This feature combination was unable to discriminate motor symptoms (see Table 1) and was a significant predictor of BIS (R^2 = 0.338, P = 0.037) but not of UPDRS (R^2 = 0.038, P = 0.72). Note that the 2 features were independent (R^2 = 0.004, P = 0.81). For ICB+ versus ICB− discrimination, the optimal point on the ROC curve of this combination of features had a specificity and sensitivity of 83.3% and 91.6%, respectively (Fig. 1D).

Discussion

We identified the subthalamic neural features displaying significant alterations associated with a high impulsivity level and leading to accurate discrimination between ICB+ and ICB− conditions. The features leading to optimal discrimination were IBF and the combination of tonic neuron fraction and SUA-BUA beta coherence. These features also significantly correlated with BIS. The possible confounding effects of motor symptoms because of UPDRS intergroup differences (-Table S1) were ruled out because they did not correlate with UPDRS or subscales and did not discriminate between patients with weak and strong motor symptoms or between patients with bradykinesia-rigid and a tremor-dominant phenotype.

Recent studies found single STN units whose firing rates were modulated with reward in decision-making tasks,[22] particularly in ICB+ patients.[12] Here we found that at rest, ICB+ and ICB− neurons do not differ in the firing rate but in the temporal structure of their

activity. Notably, these neural markers discriminated between ICB+ and ICB− patients when medication was OFF. Two factors could contribute to the differences in neural activity between the 2 groups in the OFF condition. First, DAs are not the only factor driving ICB,[3] as ICB might be associated with pretreatment differences in brain structure. Drug-naive PD patients who later developed ICBs were found to have specific neural connectivity.[23] Second, ICBs persist for months after DA discontinuation,[24] suggesting that the dopaminergic effect outlasts medication intake.[25] Moreover, the reduction in beta power and IBF and the increase in the fraction of tonic neurons we observed in ICB+ patients (see Table 1) are compatible with the hypothesis that patients developing ICB after DA treatment have a more preserved baseline state, which could be observed in the OFF medication condition.[26]

This study presents some limitations. First, this is a retrospective study. Second, we did not use the Questionnaire for Impulsive-Compulsive Disorders in the Parkinson's Disease Rating Scale[27] to discriminate between ICB+ and ICB− groups because we retrospectively collected data that predated the introduction of this scale. Third, our sample size was relatively small. Studies over a larger cohort might give a more accurate estimate of the differences between ICB+ and ICB− patients for the different features. Fourth, the limited number of neurons collected for each depth across the patients did not allow for robust statistics on the variation of features across depths. However, because the ventral region of the STN is more involved in ICB-related activity,[10,28] we might expect the distinctive features we found to be more prominent in that region.

Our results highlight for the first time the specific neural dynamics of ICB in PD in the OFF medication state, and this might have relevant clinical implications. Even if the DBS effects on ICB are still controversial,[29] there may be important differences, according to the type of DBS surgery, the active contacts, and stimulation parameters.[30] In future studies we will investigate how the online analysis of the ICB-informative neural features in MER could improve the localization of DBS electrodes[18] to treat ICB and avoid post-DBS de novo ICB. ■

Acknowledgments: We thank Prof. Marco Paganini for kindly sharing data and continuous support, Elena Vicari for contributing to the preprocessing, and Prof. Silvestro Micera for fruitful discussions.

REFERENCES

1. Erga AH, Alves G, Larsen JP, Tysnes OBR, Impulsive PKF. Compulsive behaviors in Parkinson's disease: the Norwegian ParkWest study. J Parkinsons Dis 2017;7(1):183–191.
2. Baig F, Kelly MJ, Lawton MA, et al. Impulse control disorders in Parkinson disease and RBD: a longitudinal study of severity. Neurology 2019;93(7):e675–e687.
3. Weintraub D, Koester J, Potenza MN, et al. Impulse control disorders in Parkinson disease: a cross-sectional study of 3090 patients. Arch Neurol 2010;67(5):589–595.
4. Izzo VA, Donati MA, Torre E, Ramat S, Primi C. Impulse control disorders in Parkinson's disease versus in healthy controls: a different predictive model. J Neuropsychol 2020;14(2):318–332.
5. Garcia-Ruiz PJ, Martinez Castrillo JC, Alonso-Canovas A, et al. Impulse control disorder in patients with Parkinson's disease under dopamine agonist therapy: a multicentre study. J Neurol Neurosurg Psychiatry 2014;85(8):840–844.
6. Rossi PJ, de Jesus S, Hess CW, et al. Measures of impulsivity in Parkinson's disease decrease after DBS in the setting of stable dopamine therapy. Parkinsonism Relat Disord 2017;44:13–17.
7. Weintraub D. Impulse control disorders in Parkinson's disease: a 20-year odyssey. Mov Disord 2019;34(4):447–452.
8. Jahanshahi M, Obeso I, Baunez C, Alegre M, Krack P. Parkinson's disease, the subthalamic nucleus, inhibition, and impulsivity. Mov Disord 2015;30(2):128–140.
9. Jahanshahi M, Obeso I, Rothwell JC, Obeso JA. A fronto-striato-subthalamic-pallidal network for goal-directed and habitual inhibition. Nat Rev Neurosci 2015;16(12):719–732.
10. Rodriguez-Oroz MC, López-Azcárate J, Garcia-Garcia D, et al. Involvement of the subthalamic nucleus in impulse control disorders associated with Parkinson's disease. Brain 2011;134(1):36–49.
11. Mazzoni A, Rosa M, Carpaneto J, Romito LM, Priori A, Micera S. Subthalamic neural activity patterns anticipate economic risk decisions in gambling. eNeuro 2018;5(1):1–17.
12. Rossi PJ, Shute JB, Opri E, et al. Impulsivity in Parkinson's disease is associated with altered subthalamic but not globus pallidus internus activity. J Neurol Neurosurg Psychiatry 2017;88(11):968–970.
13. Tekriwal A, Afshar NM, Santiago-Moreno J, et al. Neural circuit and clinical insights from intraoperative recordings during deep brain stimulation surgery. Brain Sci 2019;9(7):173.
14. Hughes AJ, Daniel SE, Kilford L, Lees AJ. Accuracy of clinical diagnosis of idiopathic Parkinson's disease: a clinico-pathological study of 100 cases. J Neurol Neurosurg Psychiatry 1992;55(3):181–418.
15. Fossati A, Di Ceglie A, Acquarini E, Barratt ES. Psychometric properties of an Italian version of the Barratt impulsiveness Scale-11 (BIS-11) in nonclinical subjects. J Clin Psychol 2001;57(6):815–828.
16. Cieciersky K, Mndat T, Rola R, Ras ZW, Przybyszewsky AW. Computer aided subthalamic nucleus (STN) localization during deep brain stimulation (DBS) surgery in Parkinson's patients. Ann Acad Med Silesiensis 2014;68(5):275–283.
17. Chaure FJ, Rey HG, Quian Quiroga R. A novel and fully automatic spike-sorting implementation with variable number of features. J Neurophysiol 2018;120(4):1859–1871.
18. Vissani M, Cordella R, Micera S, Eleopra R, Romito LM, Mazzoni A. Spatio-temporal structure of single neuron subthalamic activity identifies DBS target for anesthetized Tourette syndrome patients. J Neural Eng 2019;16(6):066011.
19. Shimazaki H, Shinomoto S. Kernel bandwidth optimization in spike rate estimation. J Comput Neurosci 2010;29(1–2):171–182.
20. Gourévitch B. Eggermont JJ. A nonparametric approach for detection of bursts in spike trains. J Neurosci Methods 2007;160(2):349–358.
21. Matzner A, Bar-Gad I. Quantifying spike train oscillations: biases, distortions and solutions. PLoS Comput Biol 2015;11(4):e1004252.
22. Justin Rossi P, Peden C, Castellanos O, Foote KD, Gunduz A, Okun MS. The human subthalamic nucleus and globus pallidus internus differentially encode reward during action control. Hum Brain Mapp 2017;38(4):1952–1964.
23. Tessitore A, De Micco R, Giordano A, et al. Intrinsic brain connectivity predicts impulse control disorders in patients with Parkinson's disease. Mov Disord 2017;32(12):1710–1719.
24. Corvol J-C, Artaud F, Cormier-Dequaire F, Rascol O, Durif F, Derkinderen P, et al. Longitudinal analysis of impulse control disorders in Parkinson disease. Neurology 2018;91(3):e189–e201.
25. Eisinger RS, Ramirez-Zamora A, Carbunaru S, et al. Medications, deep brain stimulation, and other factors influencing

impulse control disorders in Parkinson's disease. Front Neurol 2019;10:86.

26. de Micco R, Russo A, Tedeschi G, Tessitore A. Impulse control behaviors in Parkinson's disease: drugs or disease? Contribution From Imaging Studies. Front Neurol 2018;9:893.
27. Weintraub D, Mamikonyan E, Papay K, Shea JA, Xie SX, Siderowf A. Questionnaire for impulsive-compulsive disorders in Parkinson's disease-rating scale. Mov Disord 2012;27(2):242–247.
28. Accolla EA, Herrojo Ruiz M, Horn A, et al. Brain networks modulated by subthalamic nucleus deep brain stimulation. Brain 2016; 139(Pt 9):2503–2515.
29. Kurtis MM, Rajah T, Delgado LF, Dafsari HS. The effect of deep brain stimulation on the non-motor symptoms of Parkinson's disease: a critical review of the current evidence. NPJ Parkinsons Dis 2017;3:16024.
30. van Wouwe NC, Pallavaram S, Phibbs FT, et al. Focused stimulation of dorsal subthalamic nucleus improves reactive inhibitory control of action impulses. Neuropsychologia 2017;99:37–47.

Supporting Data

Additional Supporting Information may be found in the online version of this article at the publisher's web-site.

SGML and CITI Use Only
DO NOT PRINT

Authors Roles

(1) Research project: A. Conception, B. Organization, C. Execution; (2) Statistical Analysis: A. Design, B. Execution, C. Review and Critique; (3) Manuscript Preparation: A. Writing of the first draft, B. Review and Critique.

F.M.: 1A, 1B, 1C, 2B, 3A, 3B;
M.V.: 1A, 1B, 1C, 2A, 3A, 3B;
G.P.: 1C, 2C, 3B;
F.T.: 1C, 2C, 3B;
S.R.: 1A, 1B, 2C, 3A, 3B;
A.M: 1A, 1B, 2A, 2C, 3A, 3B.